EUROPEAN COMMISSION

Community research

PAMINA
Performance Assessment Methodologies in Application to Guide the Development of the Safety Case

(Contract Number: FP6-036404)

PA approaches based on different geometric complexity of modelling for the far field of a repository in salt
DELIVERABLE (D-N°:4.2.1)

Author(s): **André Rübel**

Date of issue of this report : **31/08/2009**

Start date of project : **01/10/2006** Duration : 36 Months

Project co-funded by the European Commission under the Euratom Research and Training Programme on Nuclear Energy within the Sixth Framework Programme (2002-2006)		
Dissemination Level		
PU	Public	X
RE	Restricted to a group specified by the partners of the [PAMINA] project	
CO	Confidential, only for partners of the [PAMINA] project	

Foreword

The work presented in this report was developed within the Integrated Project PAMINA: **P**erformance **A**ssessment **M**ethodologies **IN A**pplication to Guide the Development of the Safety Case. This project is part of the Sixth Framework Programme of the European Commission. It brings together 25 organisations from ten European countries and one EC Joint Research Centre in order to improve and harmonise methodologies and tools for demonstrating the safety of deep geological disposal of long-lived radioactive waste for different waste types, repository designs and geological environments. The results will be of interest to national waste management organisations, regulators and lay stakeholders.

The work is organised in four Research and Technology Development Components (RTDCs) and one additional component dealing with knowledge management and dissemination of knowledge:

- In RTDC 1 the aim is to evaluate the state of the art of methodologies and approaches needed for assessing the safety of deep geological disposal, on the basis of comprehensive review of international practice. This work includes the identification of any deficiencies in methods and tools.

- In RTDC 2 the aim is to establish a framework and methodology for the treatment of uncertainty during PA and safety case development. Guidance on, and examples of, good practice will be provided on the communication and treatment of different types of uncertainty, spatial variability, the development of probabilistic safety assessment tools, and techniques for sensitivity and uncertainty analysis.

- In RTDC 3 the aim is to develop methodologies and tools for integrated PA for various geological disposal concepts. This work includes the development of PA scenarios, of the PA approach to gas migration processes, of the PA approach to radionuclide source term modelling, and of safety and performance indicators.

- In RTDC 4 the aim is to conduct several benchmark exercises on specific processes, in which quantitative comparisons are made between approaches that rely on simplifying assumptions and models, and those that rely on complex models that take into account a more complete process conceptualization in space and time.

The work presented in this report was performed in the scope of RTDC 4.

All PAMINA reports can be downloaded from http://www.ip-pamina.eu.


PAMINA

1. Introduction

In Performance Assessment (PA) usually highly simplified models are used in the integrated performance assessment calculations to depict the real situation - even in those cases, where more realistic approaches exist. The reasons to use highly simplified models are on the one hand to have a more transparent and traceable model and on the other hand to reduce the computing time. The latter is of special importance in situations where probabilistic assessments have to be performed with hundreds of simulations. In many cases the simplifications in the model lead to deviations of the calculated results from the simplified PA model compared to the results that would have been achieved using a more realistic model. On the one hand it always has to be ensured in PA that deviations resulting from the simplification of the model only lead to higher values of the respective safety indicator calculated (e.g. the annual dose rate), i.e. a higher degree of conservatism. On the other hand it is however desirable not to have a too high degree of conservatism in the integrated PA calculation, so that not too unrealistic results are obtained that may result in a loss of credibility. Therefore it is desirable to check from time to time whether the simplified PA models still fit the given requirements if compared to state of the art models.

In this area of conflict RTD component 4 of the project PAMINA is positioned with its objective to evaluate whether using more complex and more realistic modelling approaches with the help of actual high-performance tools

- give an account in a demonstration/trust logic with the comprehension of the process,
- provide an added value for PA, and
- are required to include processes not yet fully accounted for in PA.

The evaluations performed in RTDC 4 consist in the comparison of results from fully integrated models, from supporting numerical codes with a high level of geometrical accuracy and from usual compartmental, semi-analytical or simplified models and codes. Through different benchmark exercises on specific processes, the relevance, advantages and limitations inherent to each approach and their associated tools are assessed.

In workpackage 2 of RTDC 4, GRS examined the use of more complex far-field codes in PA. The GRS defined two generic test cases, both giving a very highly simplified representation of the situation found in the overburden above a real salt dome in Germany. For given radionuclide release rates from the near field, transport calculations were performed for both test cases, once with the PA code CHET and once with the more complex d^3f/r^3t codes. As result of these calculations, the time dependent concentrations were compared at different positions in the model to study whether the use of the more complex codes results in a reduction of conservatism and/or a better representation of the actual transport or not.

2. Used computer codes

In Germany, the program package EMOS is used for integrated performance assessment calculations for the entire repository system [1]. EMOS is a modular program package that includes different modules for each type of host rock and the different compartments of the repository system, i.e. near field, far field and biosphere. Within this package, the module CHET is available to simulate the transport of pollutants in the geosphere [7]. This module was used in the previous German safety assessments and is used to simulate the transport in a porous medium in a one-dimensional geometry taking into account advection, diffusion, dispersion, radioactive decay and retention by adsorption. The abstraction in the model CHET involves several simplifications. The most obvious applies to the geometry and is the reduction of the dimensions from three in the real system to one in the model. Others apply to transport processes: In the overburden of salt formations appear high saline waters resulting in density driven flow processes which are not regarded in the CHET code. Also transverse dispersion is only considered approximately.

Besides the simplifying PA codes, sophisticated 3D codes are existing to model the transport in porous media. At the GRS the two programs d^3f and r^3t were developed during the last few years to perform this task [2, 3]; the first one is to model the density driven flow while the second one is to model the pollutant transport. During the transport modelling with r^3t one makes use of the stationary or transient results of the d^3f simulations: i.e. the Darcy velocity and the fluid density serve as input for r^3t. Additionally, there exist pre- and post processors to handle the data and to visualize the results. The abbreviation d^3f stands for “distributed density-driven flow”, while r^3t stands for “radionuclides, reaction, retardation and transport”.

The numerical model d^3f was developed from 1994 to 1998 while r^3t was developed from 1998 until 2003. Several working groups of German or international universities were involved in the development lead-managed by GRS. Both of the codes use Finite-Volume discretisation and unstructured grids to enhance the resolution of hydrogeological heterogeneities. Adaption techniques controlled by a-posteriori error estimators are applied to the grid and the time steps to ensure the optimal length in time and space. As the most effective solvers for large and sparse systems of equations multigrid algorithms are taken. Additionally the entire codes are parallelised so that they can be run on workstations, PCs, cluster of PCs, and massively parallel computers, too.

The overall objective of the r^3t project was the development of a computer code to simulate pollutant transport which meets the following demands: simulation of three-dimensional transport through porous or equivalently porous media, treatment of spacious and heterogeneous areas and anisotropy, consideration of advection, element-specific diffusion, dispersion, element specific porosity and interaction processes which are relevant to long-term safety analysis, applicability for radionuclide migration as well as for chemotoxical pollutants.

In addition, for radionuclides the decay is considered within decay chains. Hence, transport simulations of various radionuclides cannot be independently performed, since isotopes affect each other. The individual interaction processes which affect the pollutants transport are given in the following: equilibrium and kinetically controlled sorption, both linear (Henry) and nonlinear (Langmuir, Freundlich), respectively; precipitation and diffusion into immobile porewater; complexation; colloidal transport and matrix diffusion via effective parameters.

3. Description of the test cases

Both test cases used by GRS in workpackage 4.2 are abstractions of the hydrogeology situation above the salt dome in Gorleben in Northern Germany. The hydrogeological situation in this area was intensively investigated by a large research programme and the results are described in [5]. Figure 1 shows a cross section from North to South through the uppermost 450 m of the overburden above the salt dome Gorleben. The top of the salt dome is indicated by the blue hatched are in the centre of figure 1. The surface of the Rupel Clay is the basis of the regional groundwater flow system. Tertiary and quaternary sediments form an up to 430 m thick system of aquifers and aquitards. In large parts of the area, the system shows a distinct layered structure that consists of two aquifers, separated by an aquitard. While the upper aquifer mainly consists of Saalian and Weichselian sediments, the lower aquifer consists of Tertiary and Elsterian sediments. The aquitard consists mainly of either the Quaternary Lauenburger Clay Complex or the Tertiary Hamburg Clay. In the northern and southern regions, the upper and the lower aquifer are in direct contact. Also in the rest of the investigation area gaps do exist in the aquitard separating the upper from the lower aquifer.

Directly above the salt dome, the Gorleben Cannel is found which has formed during the Elsterian cold stage. The formation of the Gorleben Channel completely eroded all sediments of Tertiary age and older. Loose sediments are therefore found directly above the caprock of the salt dome and in some areas even directly above the Zechstein. This results in a leeching of salt from the salt dome by the groundwater passing by and consequently also leads to high salt concentrations in the groundwater in the lower aquifer of the Gorleben Channel.

Based on the sweet/saltwater distribution in the area and hydrogeological modelling, two possible transport pathways are suggested by Klinge et al. [5] for the high saline water in the lower aquifer of the Gorleben Channel. On the one hand this is a lateral outflow into the north-western rim syncline in which the waters are collected at the basis of the aquifer due to their higher density. On the other hand it is a vertical ascension of the saline waters into the upper aquifer due to locally enhanced permeabilities in those areas where the separating aquitard is either missing or of less thickness.

A highly simplified cross section was proposed in Klinge et al. [5] and is shown in figure 2. This simplified cross section was used as a basis for the construction of a model by Flügge [4] that was used again as geometry for the simplified test case in the following.

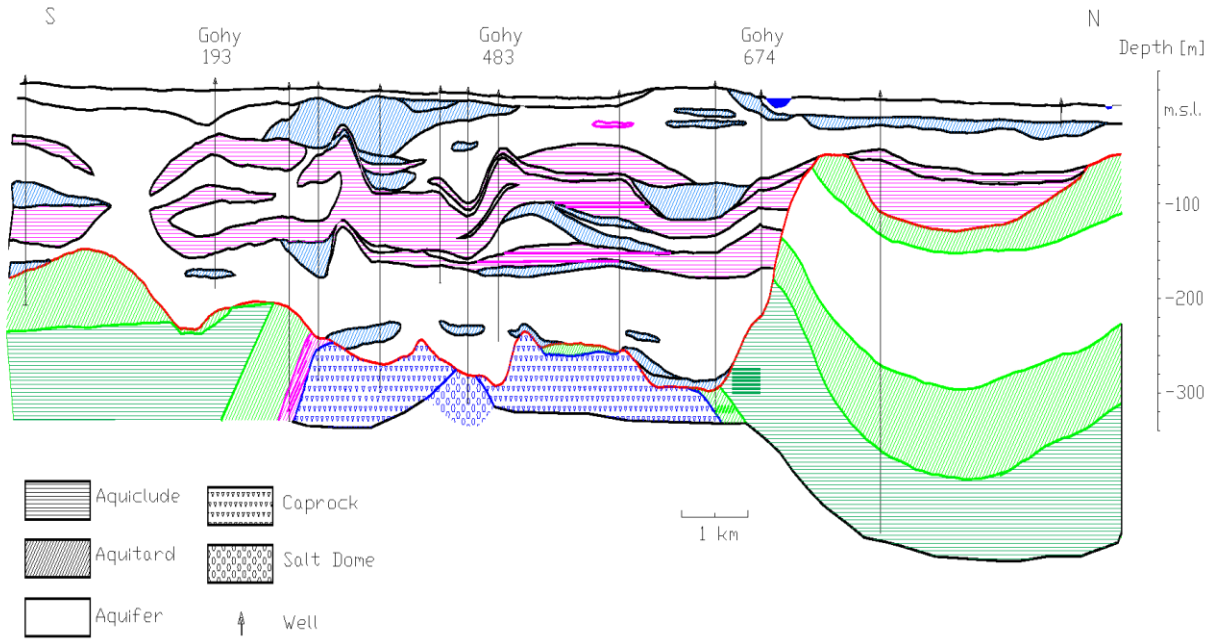

Fig. 1: Geological cross section above the Gorleben salt dome in Northern Germany [8].

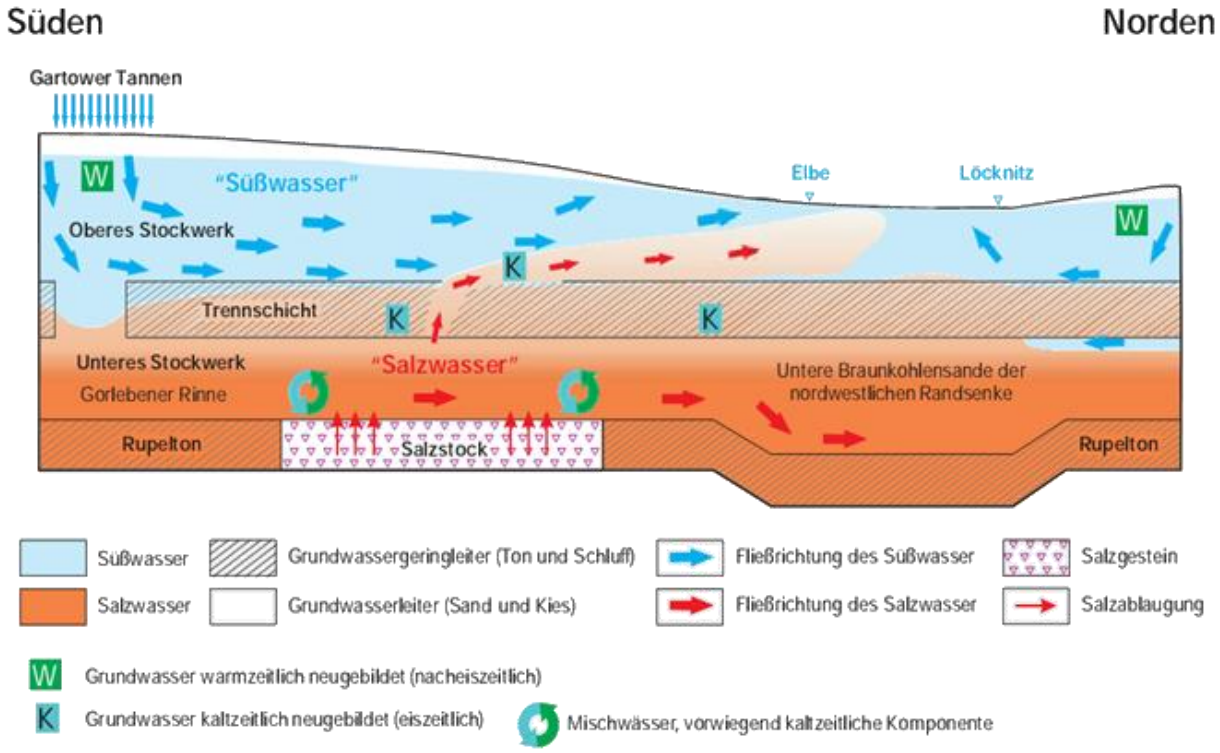

Fig. 2: Simplified cross-section [5]

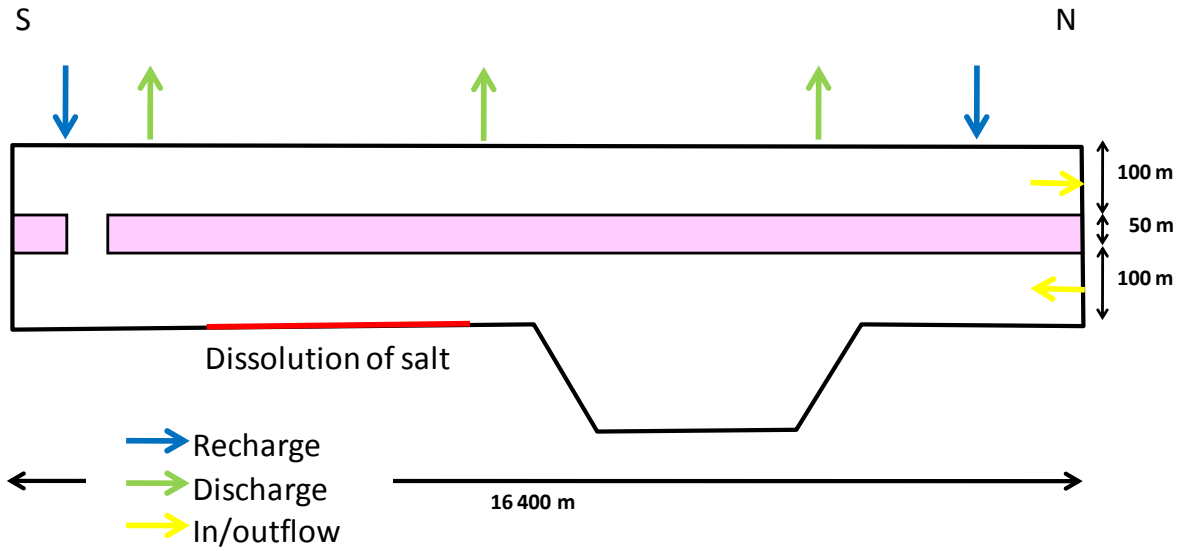

Fig. 3: Model representation of the cross section shown in figure 2.

The model used is shown in figure 3. The length of the model is 16.4 km and the height is 400 m. The overburden is divided in three horizontal layers; two aquifers on the top and on the bottom are horizontally separated by an aquiclude. Permeability values are $1 \cdot 10^{-12}$ $m^2 \cdot s^{-1}$ for the aquifer (sand) and $1 \cdot 10^{-16}$ $m^2 \cdot s^{-1}$ for the aquitard (clay). For the first model regarded in the performed calculations, the aquitard has one gap, through which water can be exchanged between both aquifers at a position of 1 000 to 1 500 m. The second model used accounts for an additional leakage at a position of 12 250 to 12 750 m. The lower aquifer is dominated by saline water, while the upper aquifer is dominated by fresh water. The salt stems from the dissolution of salt from the top of the salt dome. The dissolution of salt is simulated in the model by using a constant concentration equal to salt saturation as boundary condition at the position of 3 000 to 7 000 m, i.e. the position of the salt dome.

Water inflow occurs from the North in the lower aquifer and the inflow velocity at the boundary is set to 0.2 $m \cdot a^{-1}$ in model 1 while it is set to 2 $m \cdot a^{-1}$ in model 2. Groundwater recharge in the higher situated regions of the model in the South and in the North and amounts to 160 $mm \cdot a^{-1}$. Outflow is allowed at the Northern boundary of the upper aquifer of model 1. All other boundaries are closed. The two differences in the boundary conditions of model 1 and 2 were chosen to achieve realistic sweet/saltwater distributions in the steady state flow field.

The radionuclides are released into the aquifer directly above the salt dome at a horizontal position of the model of 4 500 m. The data for the radionuclide fluxes from the near-field are taken from the study [6] and are plotted in figure 4 for the regarded radionuclides. These radionuclide fluxes were calculated for a very unlikely disturbed evolution scenario of a repository in salt. The data for K_d-values of the radionuclides in the overburden is taken from [9] and is listed in table 2 while the values of the other transport parameters are listed in table 1.

Tab. 1: Parameters of the simple model

Parameter		Value
Geometry of the model		
Length	[m]	16 400
Height	[m]	400
Depth of sink	[m]	150
Thickness of lower aquifer	[m]	100
Thickness of aquitard	[m]	50
Thickness of upper aquifer	[m]	100
Leakage in aquitard at position	[m]	1 000 - 1 500
Additional leakage in model 2	[m]	12 250 - 12 750
Hydrogeological parameters		
Permeability of aquifer (sand)	[$m^2 \cdot s^{-1}$]	$1 \cdot 10^{-12}$
Permeability of aquitard (clay)	[$m^2 \cdot s^{-1}$]	$1 \cdot 10^{-16}$
Porosity		0.1
Longitudinal dispersivity	[m]	10
Horizontal dispersivity	[m]	1
Diffusion coefficient	[$m^2 \cdot s^{-1}$]	$1 \cdot 10^{-9}$
Boundary conditions		
Inflow in lower aquifer (model1)	[$mm \cdot a^{-1}$]	200
Inflow in lower aquifer (model2)	[$mm \cdot a^{-1}$]	2 000
Recharge	[$mm \cdot a^{-1}$]	160

Tab. 2: Kd-values for the radionuclides in the far-field [9]

Element	Sand	Clay	Element	Sand	Clay
C	$2{,}0\cdot10^{-4}$	0,002	Cs	0,07	0,4
Cl	$1{,}0\cdot10^{-4}$	$1{,}0\cdot10^{-4}$	Ra	0,04	0,3
Ni	0,02	0,3	Th	0,2	2,0
Se	0,001	0,001	Pa	0,6	60,0
Zr	0,04	0,1	U	0,002	0,08
Mo	0,001	0,001	Np	0,01	0,3
Tc	0,001	0,006	Pu	0,1	3,0
Sn	0,04	0,1	Am	0,1	20,0
I	0,002	0,002	Cm	0,1	20,0

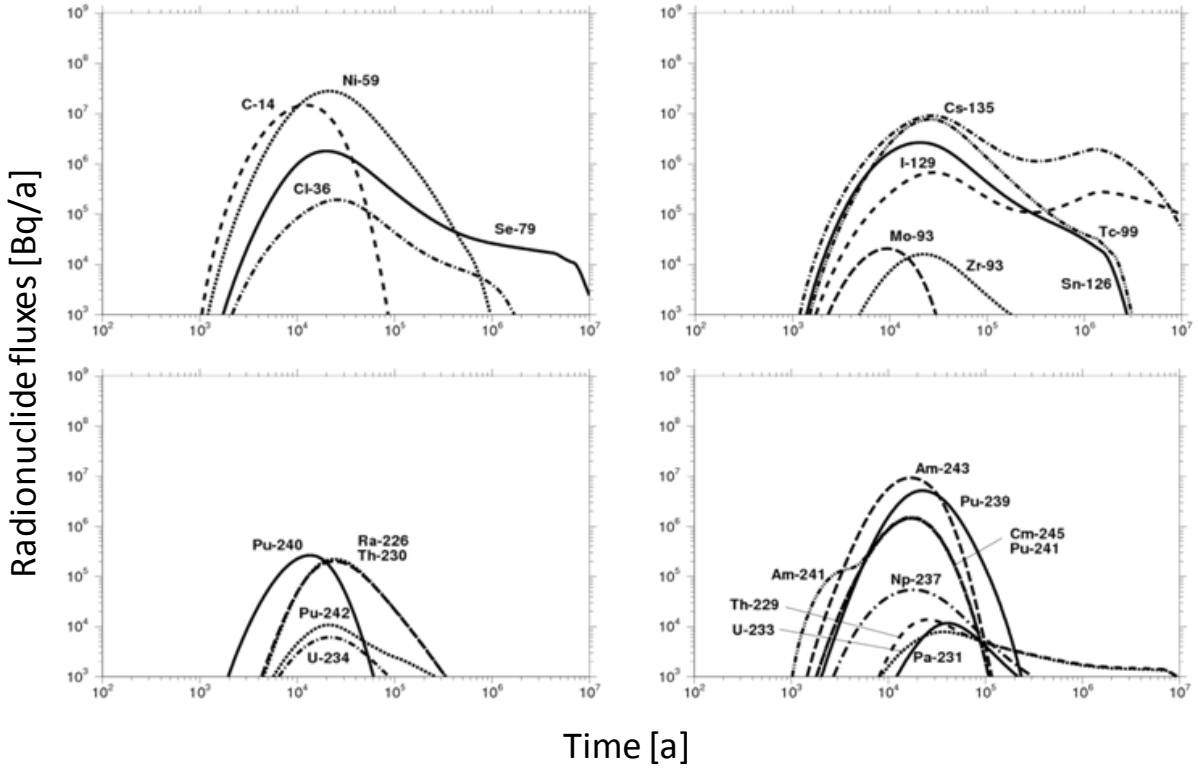

Fig. 4: Radionuclide fluxes from the near-field for the activation- and fission products (upper row) and for the decay chains (lower row).

4. Groundwater flow model results

As first step, a simulation of the density driven flow with the code d^{3}f has been performed for both models to determine the steady state flow field of water in the aquifers. The resulting flow fields are shown in figure 5 for model 1 and figure 6 for model 2 along with the salt concentration in the system. The arrows indicate the flow direction of the water while the colour coding denotes the salt concentration given in relative units compared to saturation.

For the following simulations, these flow fields were used on the one hand as direct input parameter for the transport calculations with the detailed transport code r^{3}t and in a second step to determine mean ground water velocities for the simulation with the integrated one-dimensional code CHET for the preferential transport paths identified in the transport simulations with r^{3}t.

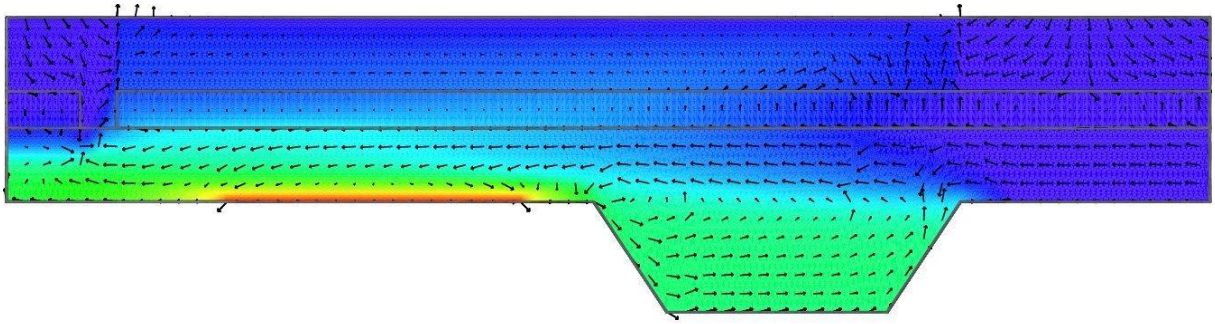

Fig. 5: Steady-state flow field for model 1. The colour scale denotes the salt concentration relative to saturation while the arrows denote the flow field.

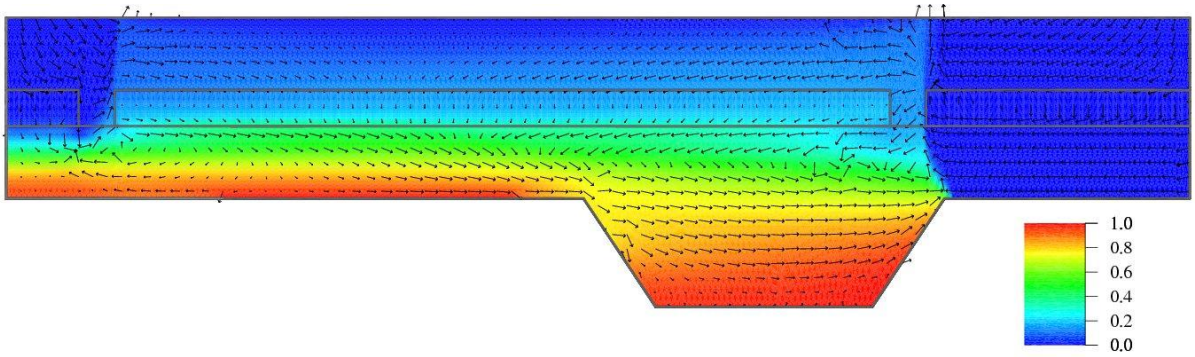

Fig. 6: Steady-state flow field for model 2. The colour scale denotes the salt concentration relative to saturation while the arrows denote the flow field.

5. 2D transport model results

The radionuclide transport was modelled with the transport code r^3t using the flow field determined in the density driven flow simulations performed before. The radionuclides were released into the model at a horizontal position of 4 500 m at the bottom of the model. The temporal evolution of the radionuclide release is plotted in figure 4. The transport calculation was performed for selected fission and activation products as well as for the Uranium decay series.

The results of the transport calculations with r^3t are presented for exemplary radionuclides in terms of cross sections of the concentration distributions of the radionuclides. The figures show the concentrations in Becquerel per cubic metre of water, colour coded on a logarithmic scale ranging from 10^{-15} to 1 Bq/m^3. Note that the numbers given on the colour bar give the according exponent. The concentration distribution is shown for four different points in time demonstrating the propagation of the radionuclide plume.

The further procedure is as follows: The 2D concentration distributions are used to find the position or positions of maximum concentration at the top of the model – i.e. the maxima of potential radiation exposure of the population if the groundwater is used for drinking or other purposes. Those positions are used as observation points for the comparison with the simplified 1D model in terms of curves of radionuclide concentration versus time at these positions. The preferential flow paths from the release point to the observation point is determined visually from the 2D concentration distributions.

5.1 Model 1

The results of the transport calculations for model 1 are plotted for the radionuclides C-14, Th-230 and Ra-226 in figures 7 to 9. For C-14, the concentration is completely vanishing for times later than 500 000 years due to radioactive decay. Therefore, no concentrations are plotted for late times. For Th-230 and Ra-226, the radionuclide plume is propagating until one million of years. This is due to radioactive production of these two radionuclides by long-lived mother radionuclides in the Uranium decay chain.

It can be clearly seen from most of the pictures - e.g. in figure 7 showing the plume of C-14 for a point in time of 10 000 years - that there are two distinct preferential flow paths for the radionuclides in the overburden. The first flow path is from the point of the radionuclide release in direct vertical direction through the lower aquifer, the clay aquitard and the upper aquifer. The second flow path is first directed southwards in horizontal direction in the lower aquifer towards the gap in the clay aquitard and than through the gap into the upper aquifer and to the surface.

The radionuclides are transported in different fractions on the two pathways - depending on their adsorption behaviour. While a high fraction of a low sorbing radionuclide like C-14 is

directly transported upwards on pathway 1, the highly sorbing radionuclides like Th-230 have only a very limited ability to be transported through the clay layer, but get sorbed within.

Figure 10 shows the concentration of different radionuclides at the top of the model plotted versus the distance from the left model boundary to find the positions of maximum concentration. The different line styles denote different points in time.

All radionuclides show two distinct concentration maxima, one at about 1 600 m and another at about 4 000 m. The position of the two maxima only slightly changes with time. Therefore, these two positions are used in the following as observation points for the comparison between the 2D and the 1D simulation. The radionuclide concentration of different radionuclides at the two observation points at 1 600 m and 4 000 m as calculated by the 2D model from r^3t are shown in figure 11.

For all plotted radionuclides, the concentration at the position of 1 600 m, i.e. the radionuclides which were transported on pathway 2, reach a higher maximum concentration and also at an earlier point in time compared to the maximum concentration of the same radionuclide at the position of 4 000 m. However, while the difference of the maximum value between both positions is several orders of magnitude for C-14, the difference is only small for Cl-36. For Uranium and Thorium, the concentration given for the position at 4 000 m is not reached by vertical transport on pathway 1, but by transport on pathway 2 and a subsequent distribution of the radionuclides in the upper aquifer, as can be seen from the concentration distributions in figures 8 and 9.

Although the maximum concentration value for Cl-36 is higher resulting from radionuclides transported on pathway 2, Cl-36 show periods in time at about 200 000 a, where the concentration at the position of 4 000 m is higher than the one at position 1 600 m. This shows that for Cl-36 both pathways could potentially contribute about the same part to the radiation exposure of the population by Cl-36 if water is used from the upper aquifer. However, the transport on pathway 1 is somewhat slower, even for the low-sorbing Cl-36.

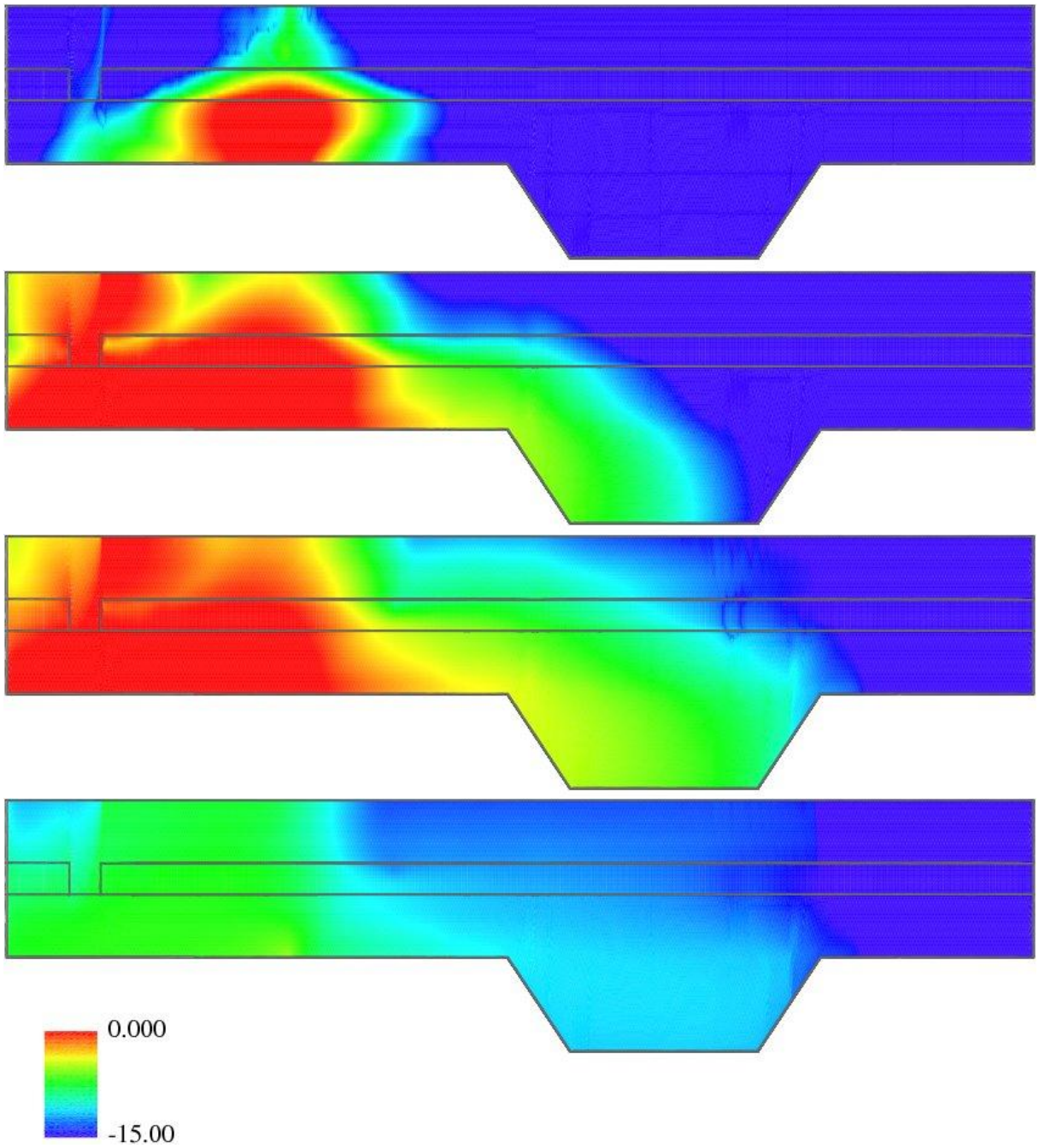

Fig. 7: Cross section of the C-14-concentration after 10 000, 50 000, 100 000 and 250 000 years in Bq/m^3. The numbers of the scale are given as common logarithm.

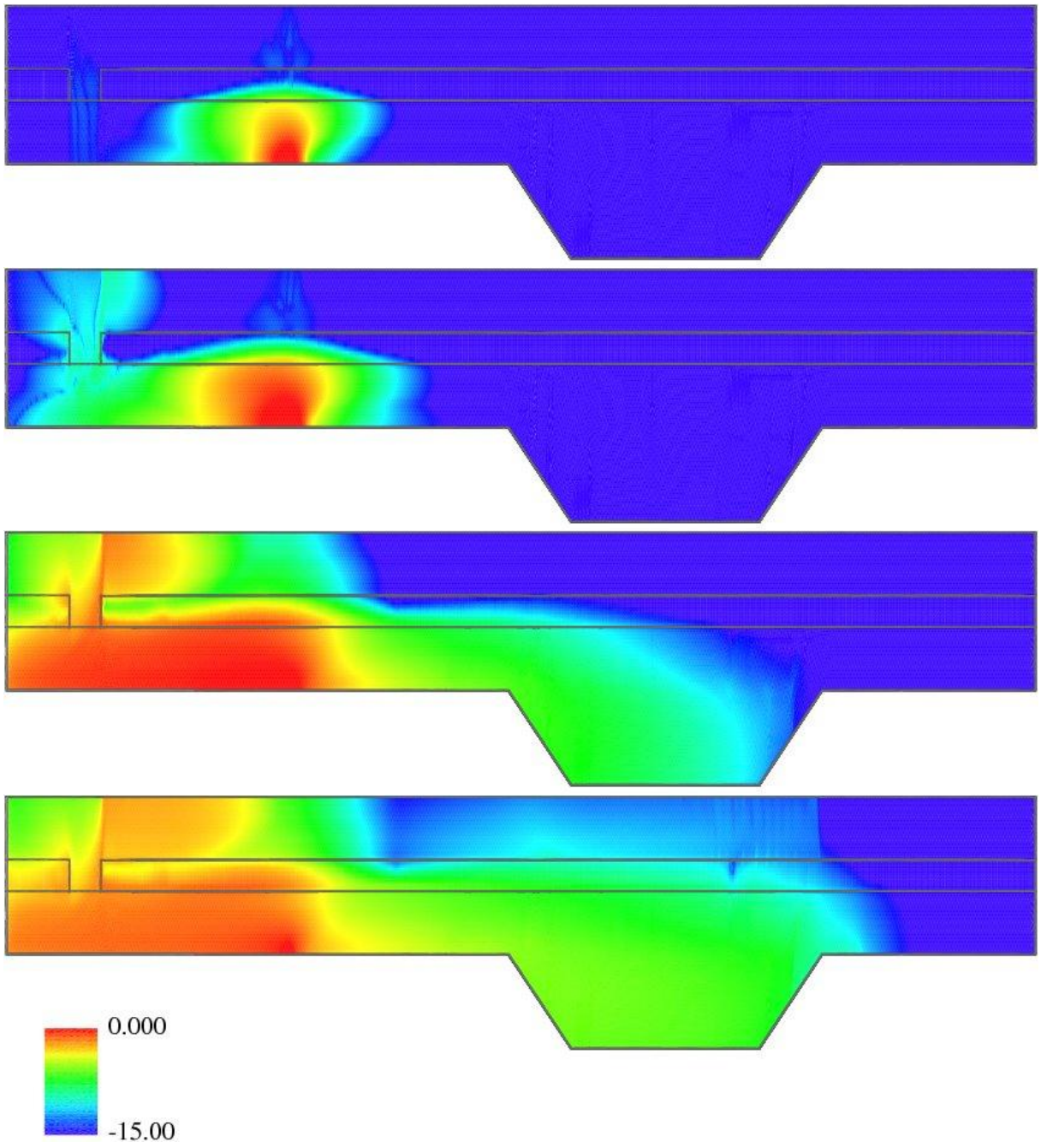

Fig. 8: Cross section of the Th-230-concentration after 50 000, 100 000, 500 000, 1 000 000 years in Bq/m^3. The numbers of the scale are given as common logarithm.

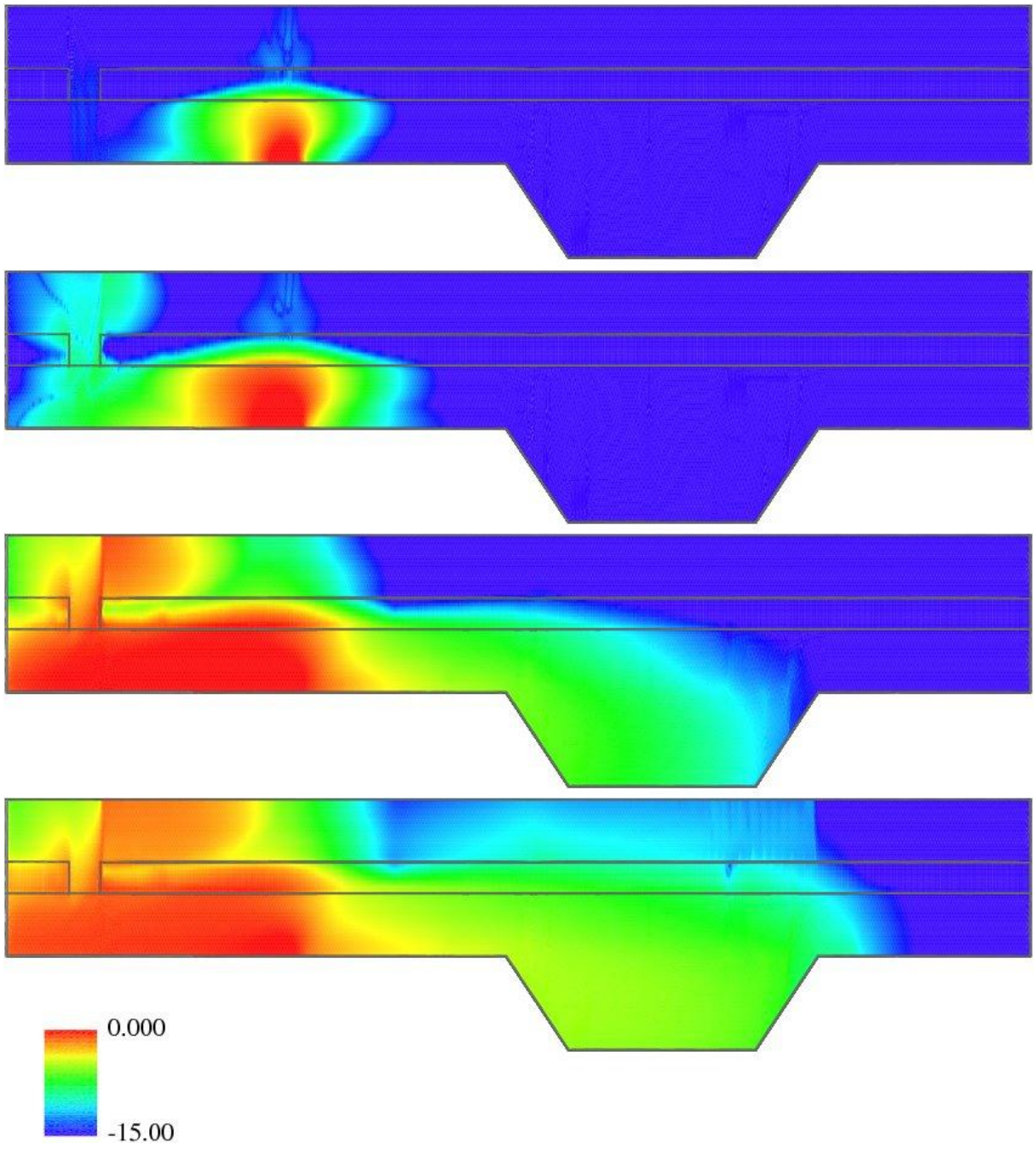

Fig. 9: Cross section of the Ra-226-concentration after 50 000, 100 000, 500 000, 1 000 000 years in Bq/m^3. The numbers of the scale are given as common logarithm.

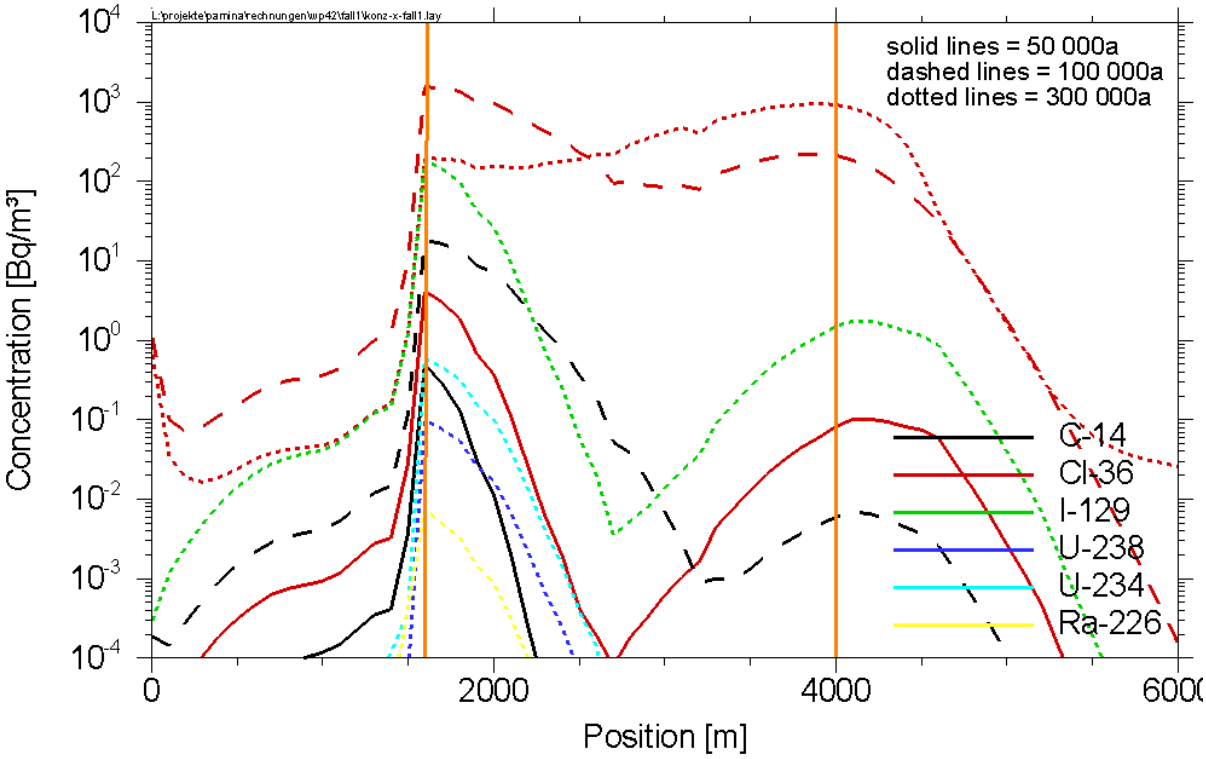

Fig. 10: Concentration of different radionuclides at the top of the model versus position

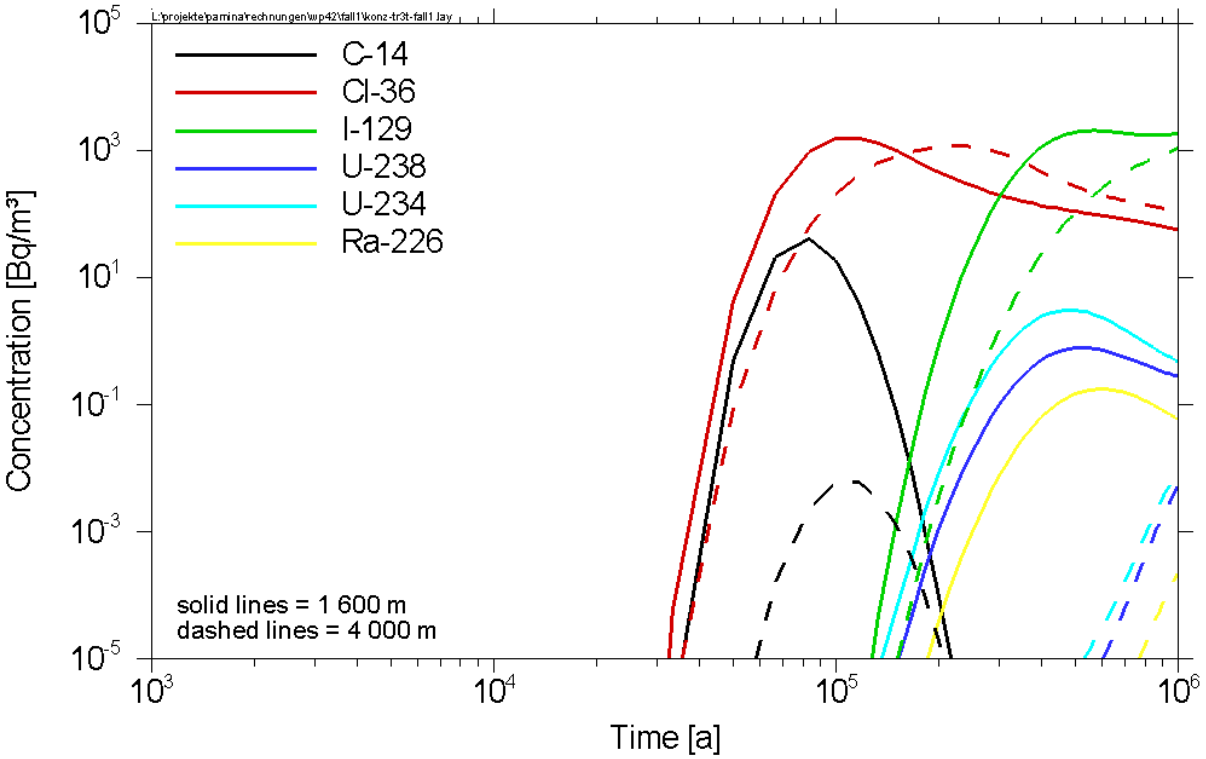

Fig. 11: Concentration of different radionuclides at position of 1 600 m (solid lines) and 4 000 m (dashed lines) at the top of the model

5.2 Model 2

The results of the transport calculations for model 2 are plotted for the radionuclides I-129, U-234 and Ra-226 in figures 12 to 14 for times from 10 000 to 300 000 years. For later times most of the radionuclides show a distribution more or less all over the whole model region.

Like for the model 2, there are two distinct preferential flow paths for the radionuclides in the overburden. The first flow path is from the radionuclide source in direct vertical direction through the lower aquifer, the clay aquitard and the upper aquifer. The second flow path is first northwards in horizontal direction in the lower aquifer, through the sink and than through the gap into the upper aquifer and to the surface. For some radionuclides also a third transport pathway is relevant. The third transport pathway is southwards in the lower aquifer and through the gap at 1600 m into the upper aquifer. This transport pathway can nicely be seen in figure 13 showing the distribution of the U-234 concentration for 300 000 years.

Figure 15 shows the concentration of different radionuclides at the top of the model plotted versus the distance from the left model boundary to find the positions of maximum concentration. The different line styles denote different points.

All radionuclides show two distinct concentration maxima, one at about 5 000 m and another at about 12 650 m, representing the pathways 1 and 2 as described above. Pathway 3 only plays a very minor role and is therefore not regarded further. The positions of the maxima of the first two pathways only slightly change with time. Therefore, these two positions are used in the following as observation points for the comparison between the 2D and the 1D simulation. The radionuclide concentration of different radionuclides at the two observation points at 5 000 m and 12 650 m as calculated by the 2D model from r^3t are shown in figure 16.

For all plotted radionuclides, the concentration at the position of 12 650 m, i.e. the radionuclides which were transported on pathway 2, reach a somewhat higher maximum concentration, but the differences are very small for most of the radionuclides. Also the maximum values are reached at similar times through both pathways. So none of the two pathways can be clearly identified to be a preferential pathway for the radionuclides.

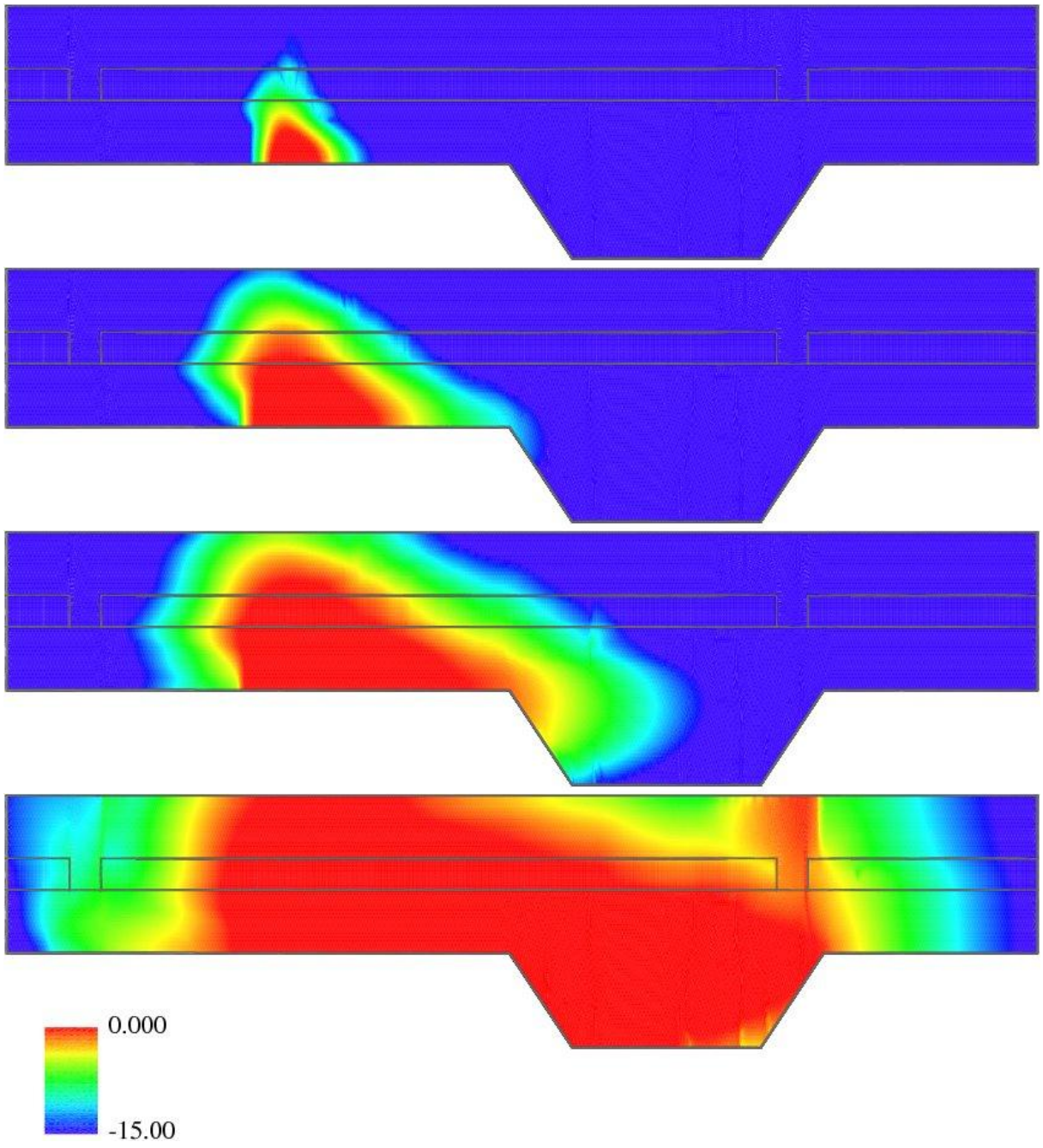

Fig. 12: Cross section of the I-129-concentration after 10 000, 50 000, 100 000, 300 000 years in Bq/m^3. The numbers of the scale are given as common logarithm.

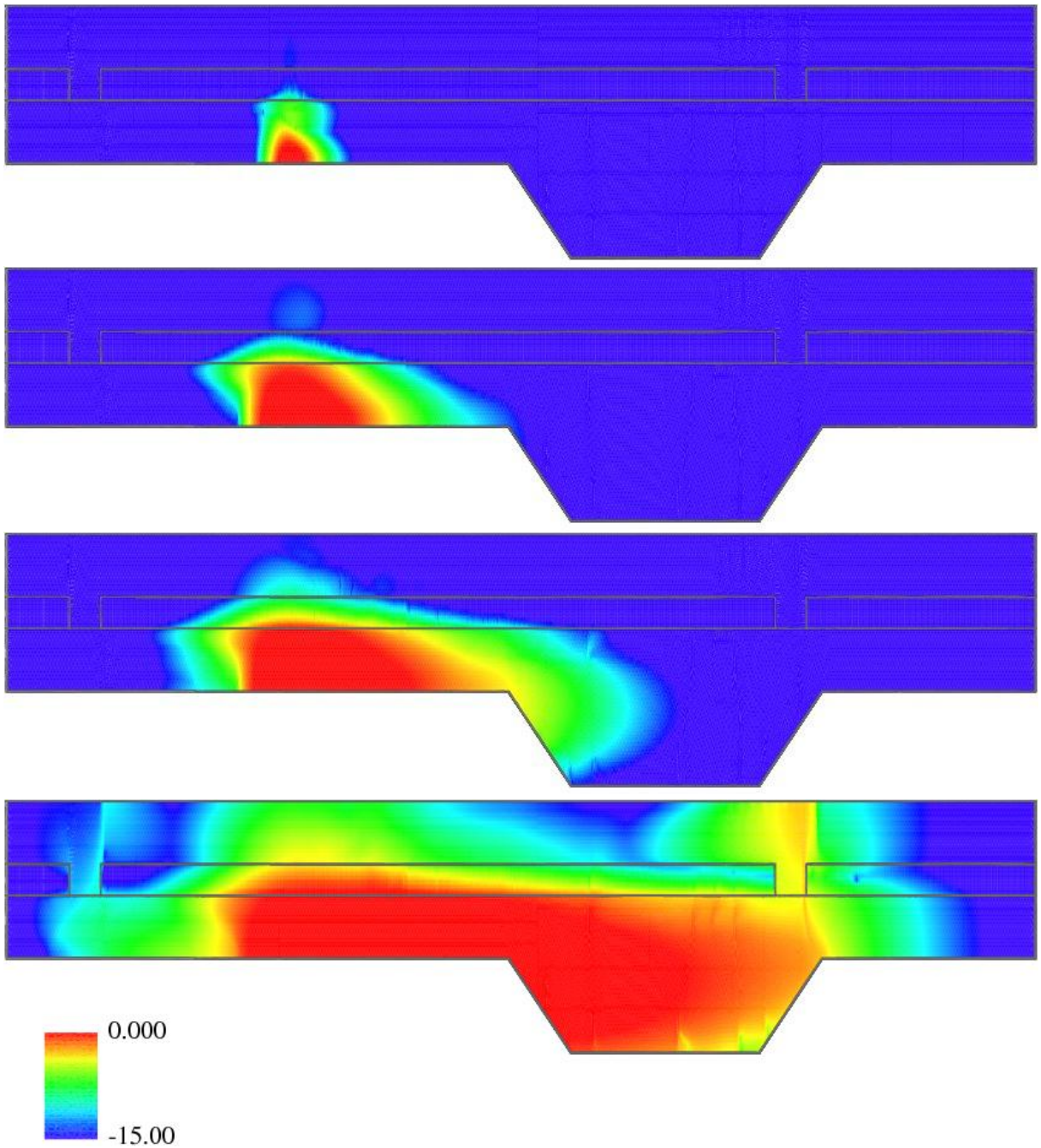

Fig. 13: Cross section of the U-234-concentration after 10 000, 50 000, 100 000, 300 000 years in Bq/m^3. The numbers of the scale are given as common logarithm.

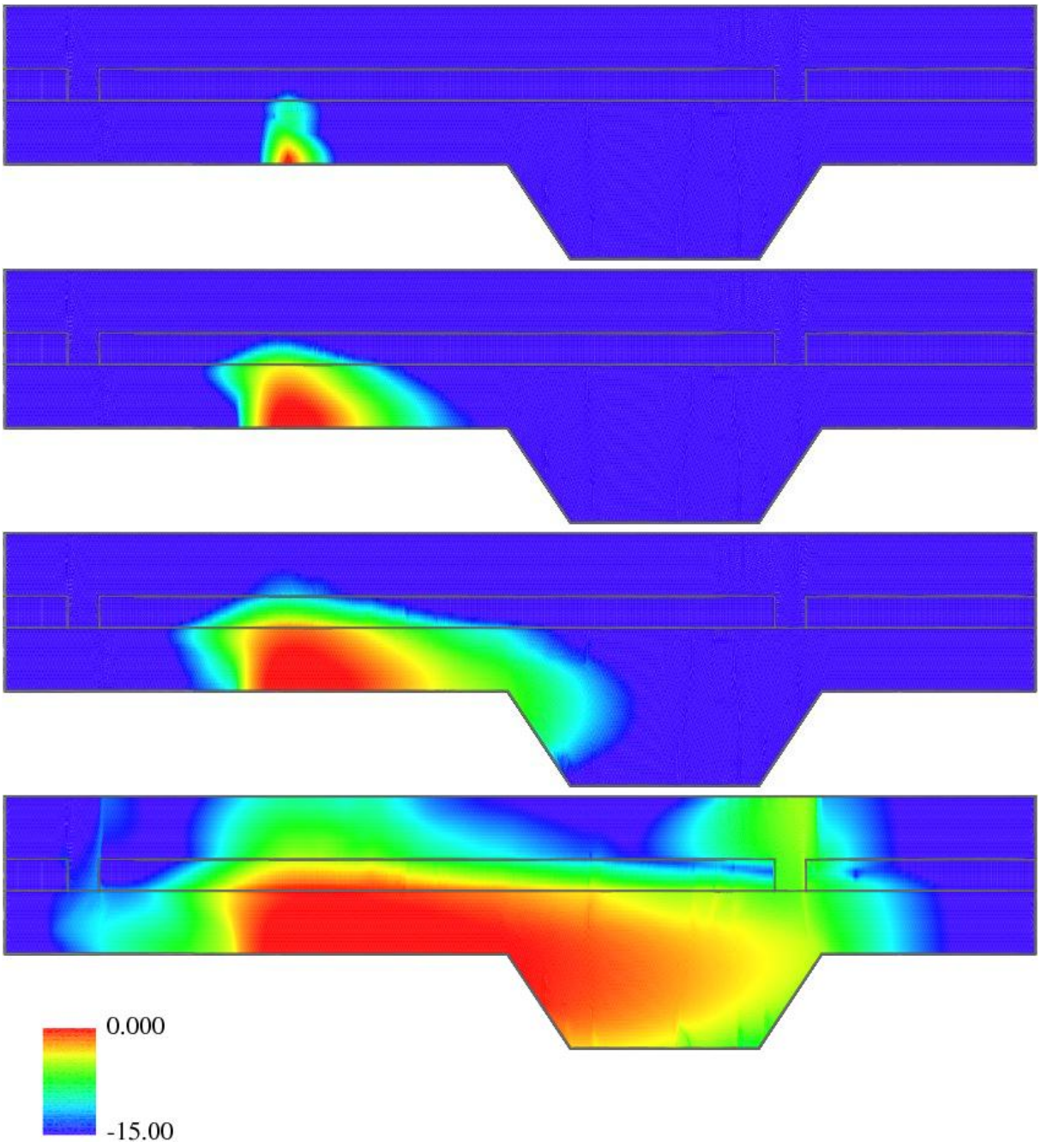

Fig. 14: Cross section of the Ra-226-concentration after 10 000, 50 000, 100 000, 300 000 years in Bq/m^3. The numbers of the scale are given as common logarithm.

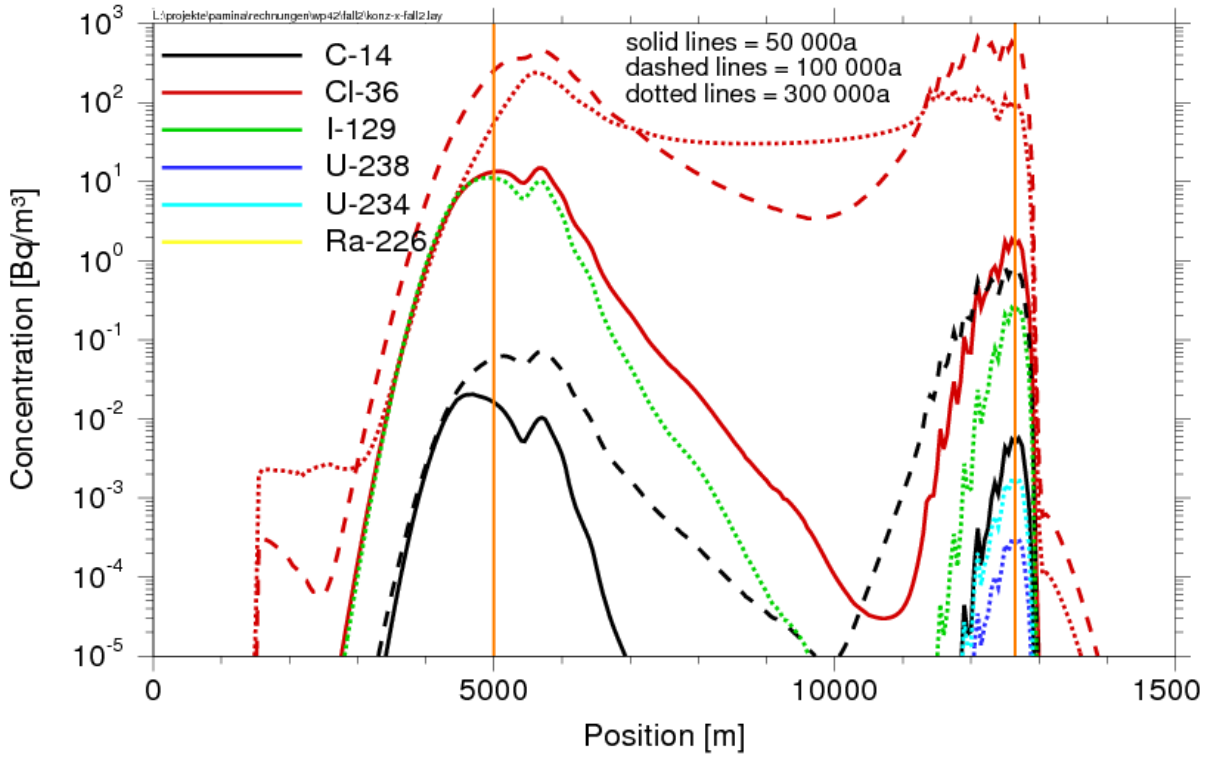

Fig. 15: Concentration of different radionuclides at the top of the model versus position

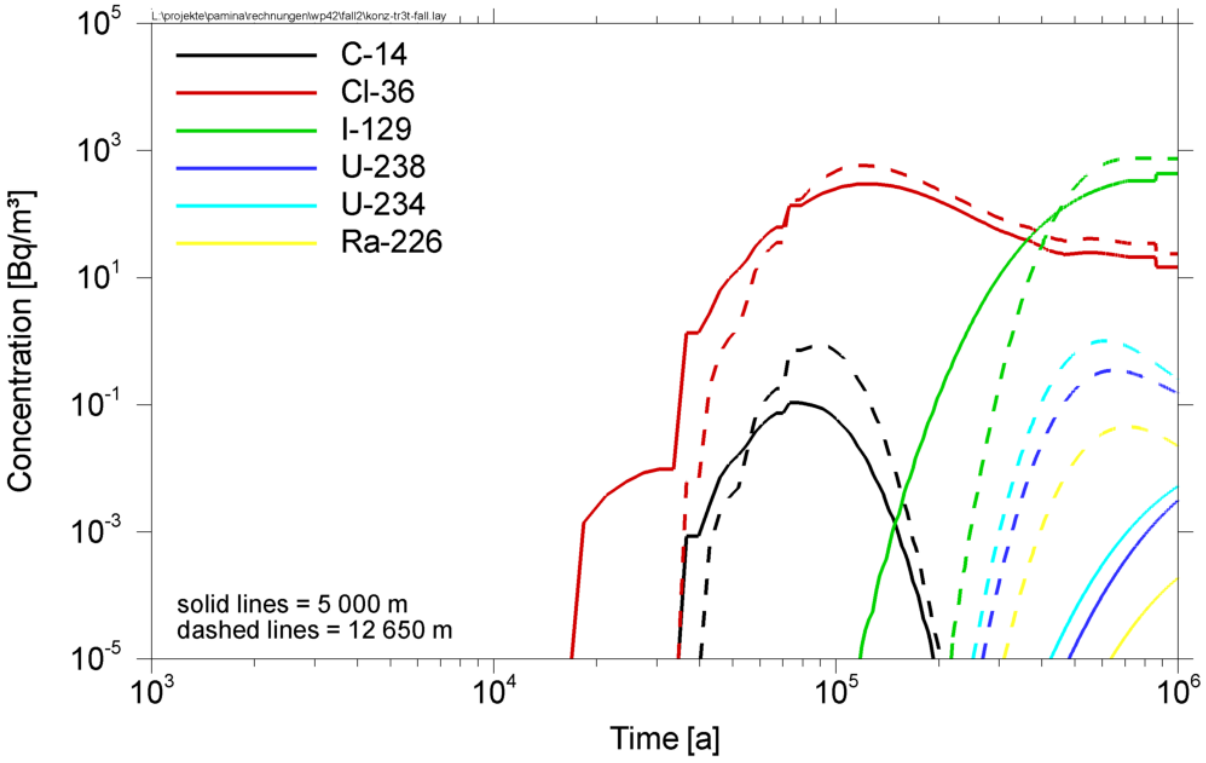

Fig. 16: Concentration of different radionuclides at position of 5 000 m (solid lines) and 12 650 m (dashed lines) at the top of the model

6. Abstraction to 1D-model

The transport on the different transport pathways identified for each of the two models above were modelled additionally with the 1D-PA-model CHET. Each of the transport pathways was divided into several modelling blocks or compartments representing either the different materials or the groundwater movement directions. The groundwater velocities needed as input parameter for the one dimensional model were derived for each compartment by averaging the ground water velocities determined in the 2D calculation with the program d^3f (figure 3) along the pathways. For the other transport and retention parameters, the same data as for the r^3t simulations was used. While the K_d-values are listed in table 2 above, the transport parameters are listed individually for each model below.

The temporal evolution of the radionuclide concentrations determined at the end of each 1D transport pathway were compared to the respective radionuclide concentrations determined for the observation points in the 2D model plotted in figures 11 and 16 above.

6.1 Model 1

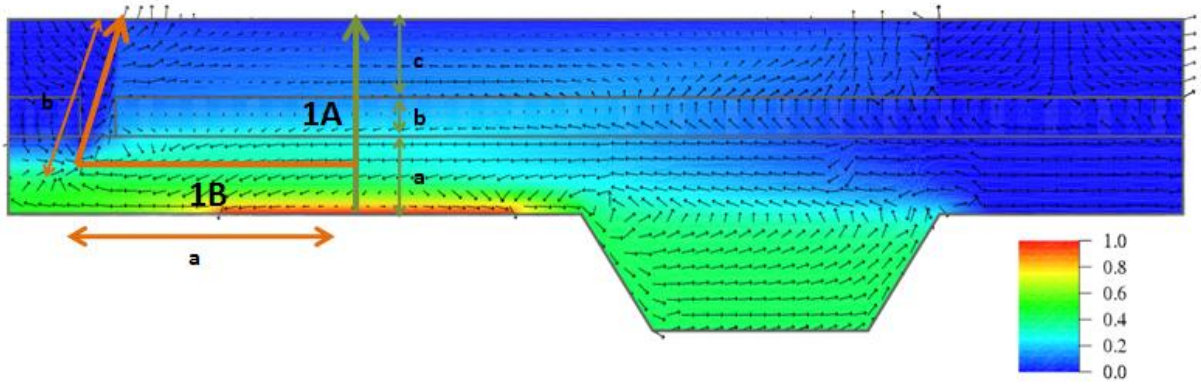

Fig. 17: Definition and subdivision of the transport pathways of model 1

Pathway A of model 1 has been divided into three sub-compartments a, b and c; the lower and upper aquifer (1Aa and 1Ac) and the aquiclude (1Ab) in between. Averaging was performed for each of the compartments individually, but it was critical for all compartments of pathway 1A due to very low or even downward directed vertical groundwater velocities. The assumed resulting groundwater velocity for all three compartments of $1 \cdot 10^{-4} m \cdot a^{-1}$ is close to expected travel velocities resulting from diffusion.

Pathway B has been divided into two sub-compartments (a and b). The first compartment (1Ba) represents the horizontal flow in the lower aquifer from the position of the radionuclide release at about 4 500 m to the position of the gap in the aquiclude at about 1 300 m. The second compartment (1Bb) comprises the vertical flow from the lower to the upper aquifer.

Tab. 3: Parameters for the 1D transport model CHET for the two transport pathways considered for model 1

Transport pathway 1A		
Number of compartments		3
Compartment 1Aa and 1Ac		
Material		Sand
Pathway length	[m]	100
Porosity		0.3
Cross section	[m^2]	1 000
Mean darcy velocity	[$m \cdot a^{-1}$]	$1 \cdot 10^{-4}$
Compartment 1Ab		
Material		Clay
Pathway length	[m]	50
Porosity		0.1
Cross section	[m^2]	1 000
Mean groundwater velocity	[$m \cdot a^{-1}$]	$1 \cdot 10^{-4}$
Transport pathway 1B		
Number of compartments		2
Compartment 1Ba		
Material		Sand
Pathway length	[m]	3 500
Porosity		0.3
Cross section	[m^2]	100
Mean groundwater velocity	[$m \cdot a^{-1}$]	$3.6 \cdot 10^{-2}$
Compartment 1Bb		
Material		Sand
Pathway length	[m]	200
Porosity		0.3
Cross section	[m^2]	200
Mean groundwater velocity	[$m \cdot a^{-1}$]	$3.15 \cdot 10^{-1}$

For the first compartment (1Ba) the horizontal flow velocity has been determined for 19 positions in x-direction at three different depth levels of the lower aquifer (175 m, 200 m and 225 m depth). The spatial variability of the groundwater velocity values is rather low and is about a factor of three between the highest and the lowest value. The average velocity determined from the mean of those 57 values is $3.6 \cdot 10^{-2}$ m·a^{-1}. For the second compartment (1Bb), the vertical velocity has been determined for three different positions in x-direction and 20 different depth levels resulting in an average velocity determined from the mean of 60 values of 0.315 m·a^{-1}. The geometric and transport parameters used for the two pathways in model 1 are summarised in table 3.

The resulting concentrations calculated in the CHET simulations are plotted in figure 18 for pathway 1A and in figure 19 for pathway 1B along with the results from r^3t presented before. The comparison results in the following observations:

- For both pathways regarded in model 1, the concentrations calculated with the CHET model are higher compared to the ones obtained by r^3t. This is true for all radionuclides shown and the difference in concentration is at least one to two orders of magnitude.

- The maximum concentrations are reached earlier in the simulations with the CHET model compared to the ones with the r^3t model. Especially for radionuclides with small half life like C-14 this difference in the travel time also results in an additional difference in the maximum concentration.

- The shape of the curves, i.e. the increase of the concentration with time for pathway A is much steeper in the results from the CHET simulation than in the results from r^3t. This is due to the fact that the vertical dispersion regarded in the 2D simulation is not included in a 1D simulation. This effect is especially visible for very slow or diffusion dominated transport – as in pathway A – since diffusive transport has no clear transport direction, but the transport velocity in direction of the pathway regarded is the same than perpendicular to it. The same difference would apply to the 2D simulation if compared to a full 3D one.

- If the curves of the radionuclides from the uranium decay chain (U-238, U-234 and Ra-226) are compared to each other for the transport on pathway B, it can be seen that the curves showing the CHET results plot farer from each other than the ones from r^3t. This indicates that the decay chain is not in radioactive equilibrium in the CHET simulation and therefore the Ra-226 concentration is underestimated. The reason for this is the high increase in the transport velocity towards the end of the transport pathway in the CHET model, and the resulting lack of time to reach the equilibrium.

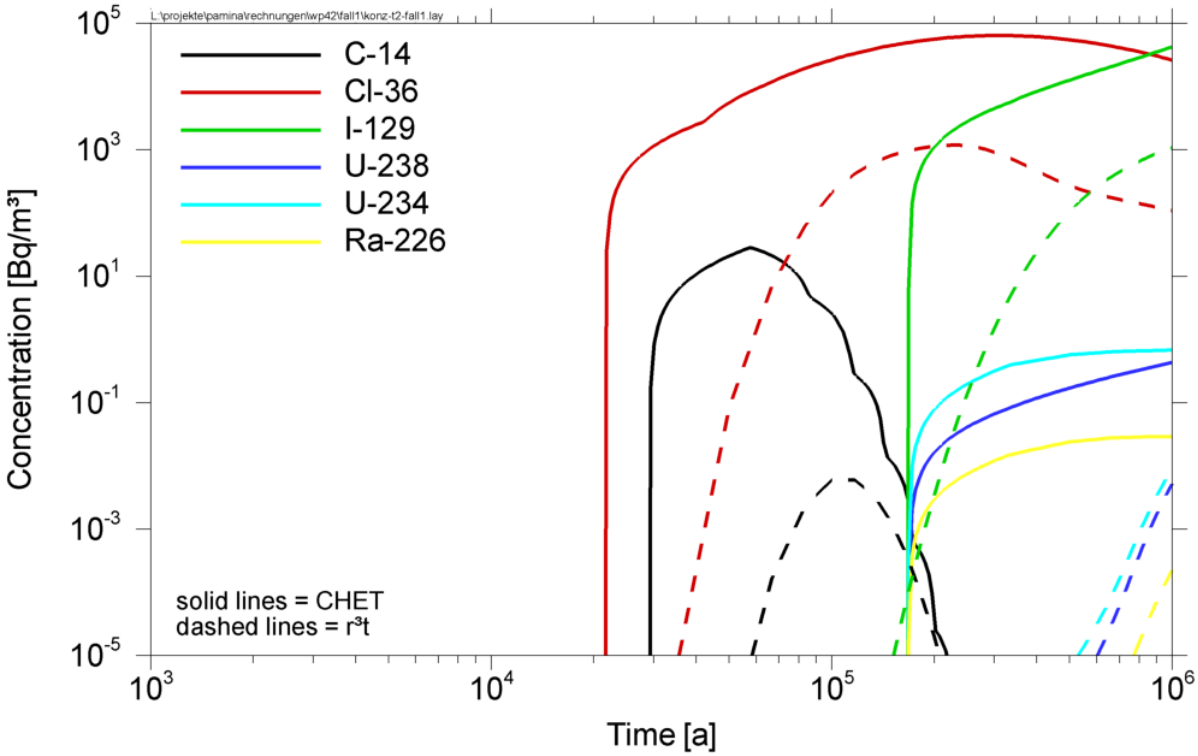

Fig. 18: Concentration versus time of different radionuclides at the position of 4 000 m (pathway 1A) calculated with r^3t (dashed lines) and CHET (solid lines)

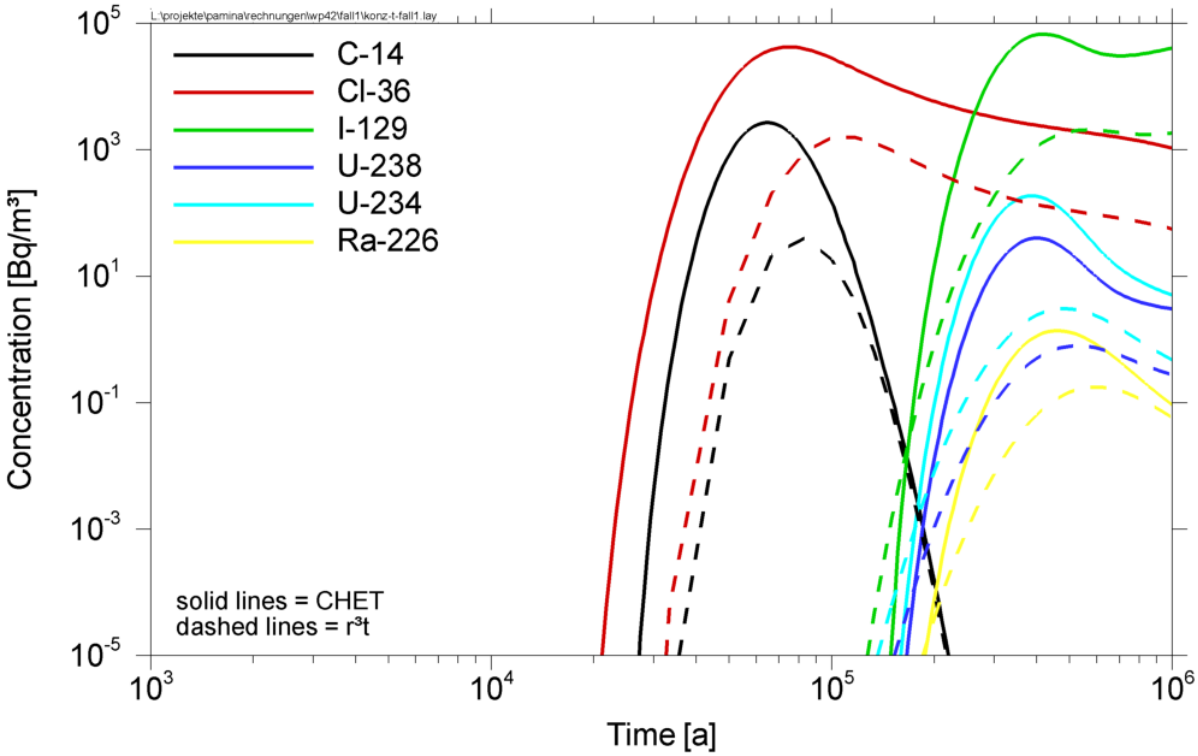

Fig. 19: Concentration versus time of different radionuclides at the position of 1 600 m (pathway 1B) calculated with r^3t (dashed lines) and with CHET (solid lines)

6.2 Model 2

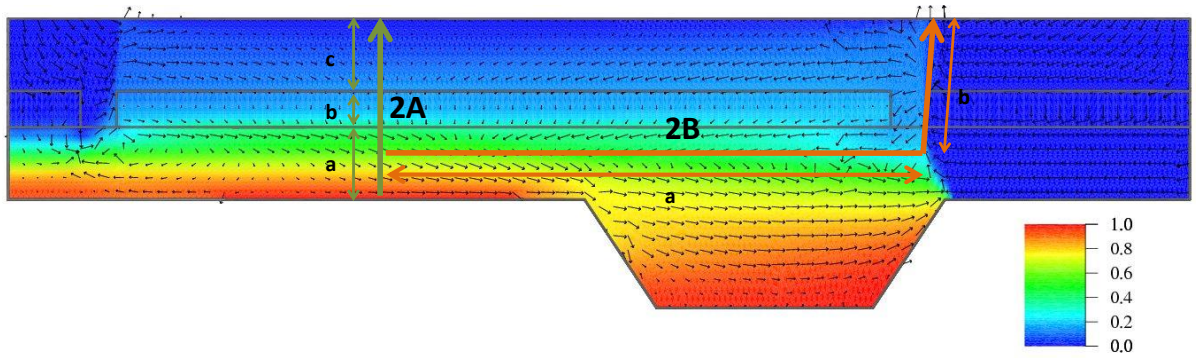

Fig. 20: Definition and subdivision of the transport pathways of model 2

Pathway A of model 2 has been handled in the same way as for model 1. It has been divided into three sub-compartments a, b and c; the lower and upper aquifer (2Aa and 2Ac) and the aquiclude (2Ab) in between. Averaging was performed for each of the compartments individually, but it was critical for all compartments. Therefore, the same resulting groundwater velocity for all three compartments of $1 \cdot 10^{-4} m \cdot a^{-1}$ was chosen as for model 1.

Pathway B has been divided into two sub-compartments (a and b). The first compartment (1Ba) represents the horizontal flow in the lower aquifer from the position of the radionuclide release at about 4 500 m to the position of the gap in the aquiclude at about 12 650 m. The second compartment (1Bb) comprises the vertical flow from the lower to the upper aquifer.

For the first compartment (2Ba), the horizontal flow velocity has been determined for 774 positions in x-direction at three different depth levels of the lower aquifer (175 m, 200 m and 225 m depth). The spatial variability of the groundwater velocity values is much higher than in the first model. In particular, there are areas where the flow velocity is negative, i.e. the local flow direction is in the opposite direction than the main flow direction. Those negative numbers were not included in the averaging. The average velocity determined is $2.1 \cdot 10^{-2}$ $m \cdot a^{-1}$. The maximum flow velocity is about a factor of 6 higher than the average.

For the second compartment (2Bb), the vertical velocity has been determined for one position in x-direction and 40 different depth levels resulting in an average velocity of 2.74 $m \cdot a^{-1}$. The geometric and transport parameters used for the two pathways in model 1 are summarised in table 3.

Tab. 4: Parameters for the 1D transport model CHET for the two transport pathways considered for model 2

Transport pathway 2A		
Number of compartments		3
Compartment 2Aa and 2Ac		
Material		Sand
Pathway length	[m]	100
Porosity		0.3
Cross section	[m^2]	1 000
Mean darcy velocity	[$m \cdot a^{-1}$]	$1 \cdot 10^{-4}$
Compartment 2Ab		
Material		Clay
Pathway length	[m]	50
Porosity		0.1
Cross section	[m^2]	1 000
Mean groundwater velocity	[$m \cdot a^{-1}$]	$1 \cdot 10^{-4}$
Transport pathway 2B		
Number of compartments		2
Compartment 2Ba		
Material		Sand
Pathway length	[m]	7 740
Porosity		0.3
Cross section	[m^2]	100
Mean groundwater velocity	[$m \cdot a^{-1}$]	$2.1 \cdot 10^{-2}$
Compartment 2Bb		
Material		Sand
Pathway length	[m]	100
Porosity		0.3
Cross section	[m^2]	100
Mean groundwater velocity	[$m \cdot a^{-1}$]	2.74

The resulting concentrations calculated in the CHET simulations are plotted in figure 21 for pathway 2A and in figure 22 for pathway 2B along with the results from r^3t. The comparison results in the following observations:

- For pathway 2A, the concentrations calculated with the CHET model are higher compared to the ones obtained by r^3t. This is true for all radionuclides shown and the difference in concentration is at least one to two orders of magnitude.

- As for model 1, the shape of the curves for very slow or diffusion controlled transport in pathway 2A is much steeper in the results from the CHET simulation than in the results from r^3t due to neglecting of vertical dispersion in the 1D model.

- For pathway 2 B, the concentrations calculated with the performance assessment model CHET are lower and occur to later times than the concentrations calculated with r^3t. Therefore, for this transport pathway the calculations with CHET are not conservative. The reason for this is the very inhomogeneous distribution of the transport velocities, resulting in too slow mean transport velocities received from the averaging. The transport velocity in x-direction of model 2 is plotted in figure 23. Red colours denote flow in positive (right) direction while blue colours denote flow in negative (left) direction. It can be seen that the flow in the lower aquifer above the sink results from two competing processes, first the convective flow from left to right (red plume) transporting the radionuclides and second, the advective inflow from the right boundary (blue plume).
  The radionuclide transport in the lower aquifer is dominated by the high transport velocity from left to right in the lower part of the lower aquifer (i.e. the centre of the red plume), while the averaging over the whole thickness of the lower aquifer results in clearly underestimated transport velocities for the radionuclides.
  If the calculation with the code CHET is repeated using the maximum transport velocity observed in the lower aquifer from left to right – which is 5.8 times higher than the average value - a result is obtained that again leads to conservative concentrations and travel times for the CHET calculation as plotted in figure 24.

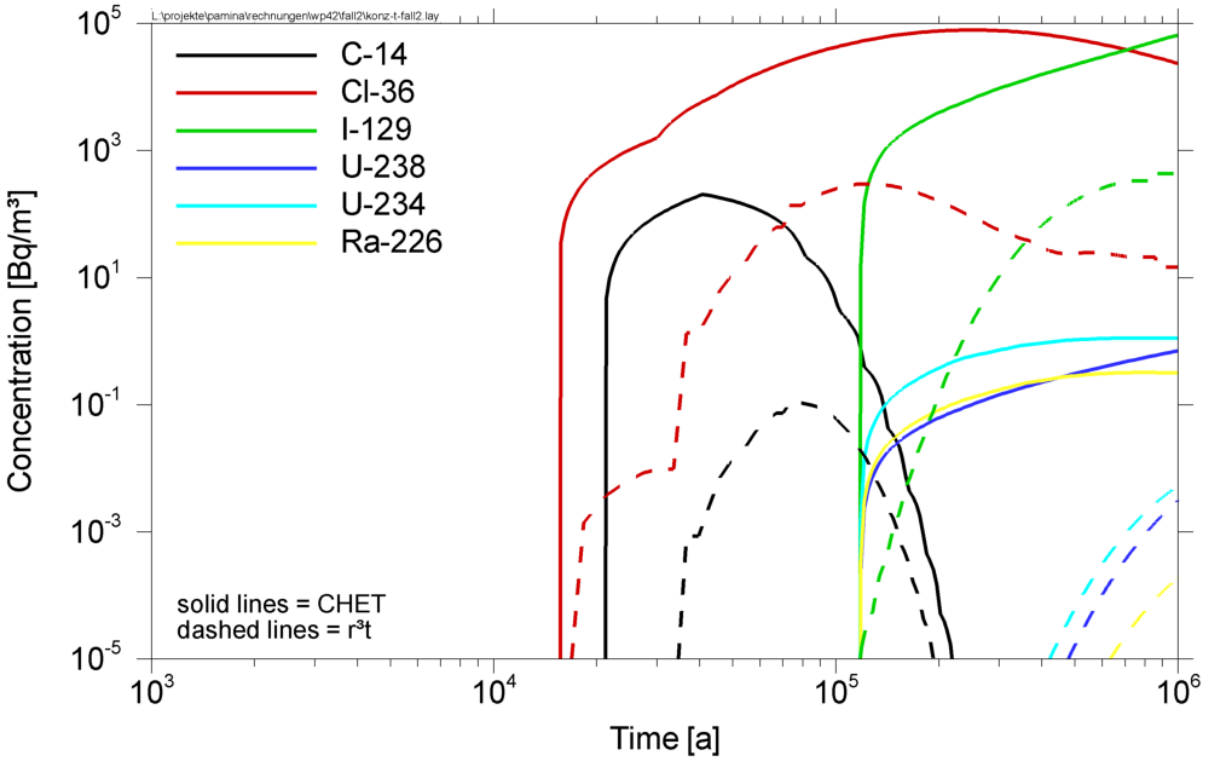

Fig. 21: Concentration versus time of different radionuclides at the position of 4 500 m (pathway 2A) calculated with r^3t (dashed lines) and CHET (solid lines) for model

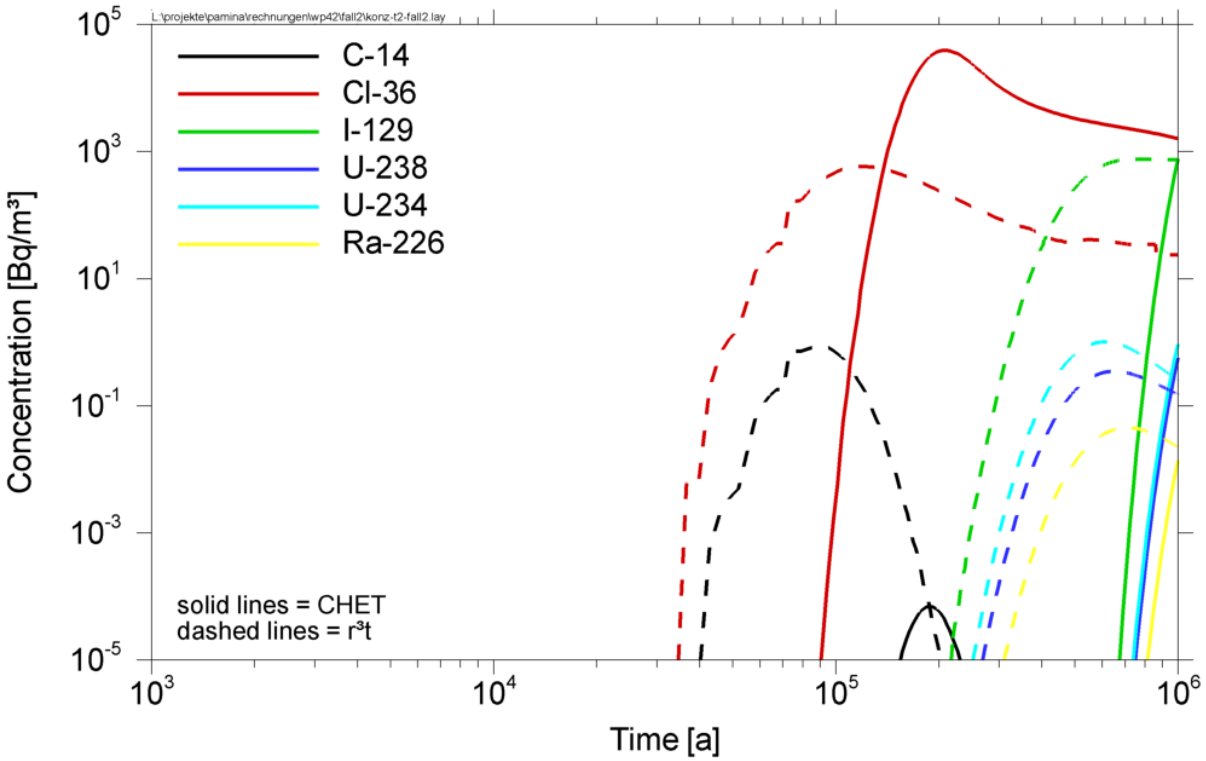

Fig. 22: Concentraton versus time of different radionuclides at the position of 12 650 m (pathway 2B) calculated with r^3t (dashed lines) and with CHET (solid lines)

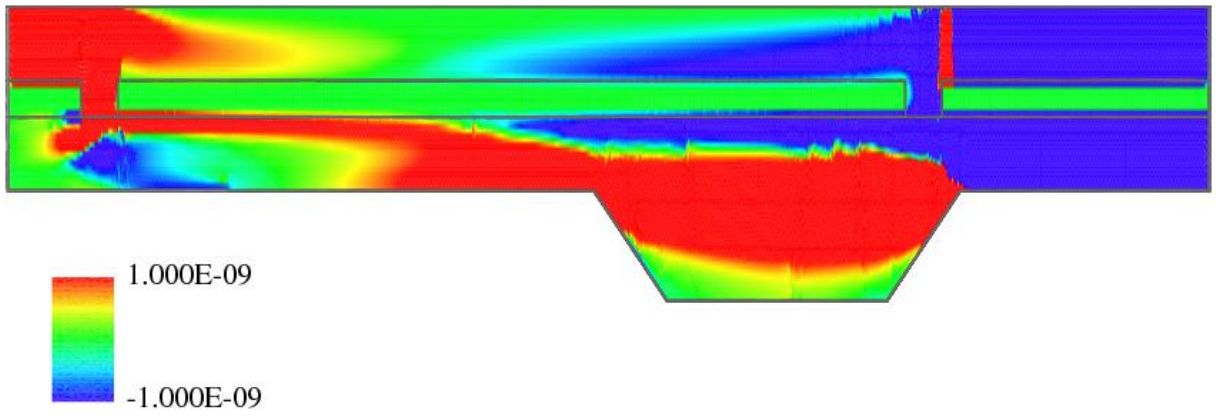

Fig. 23: Horizontal component of the flow velocity in model 2 given in [m·s^{-1}]. Red colours denote flow in positive (right) direction while blue colours denote flow in negative (left) direction.

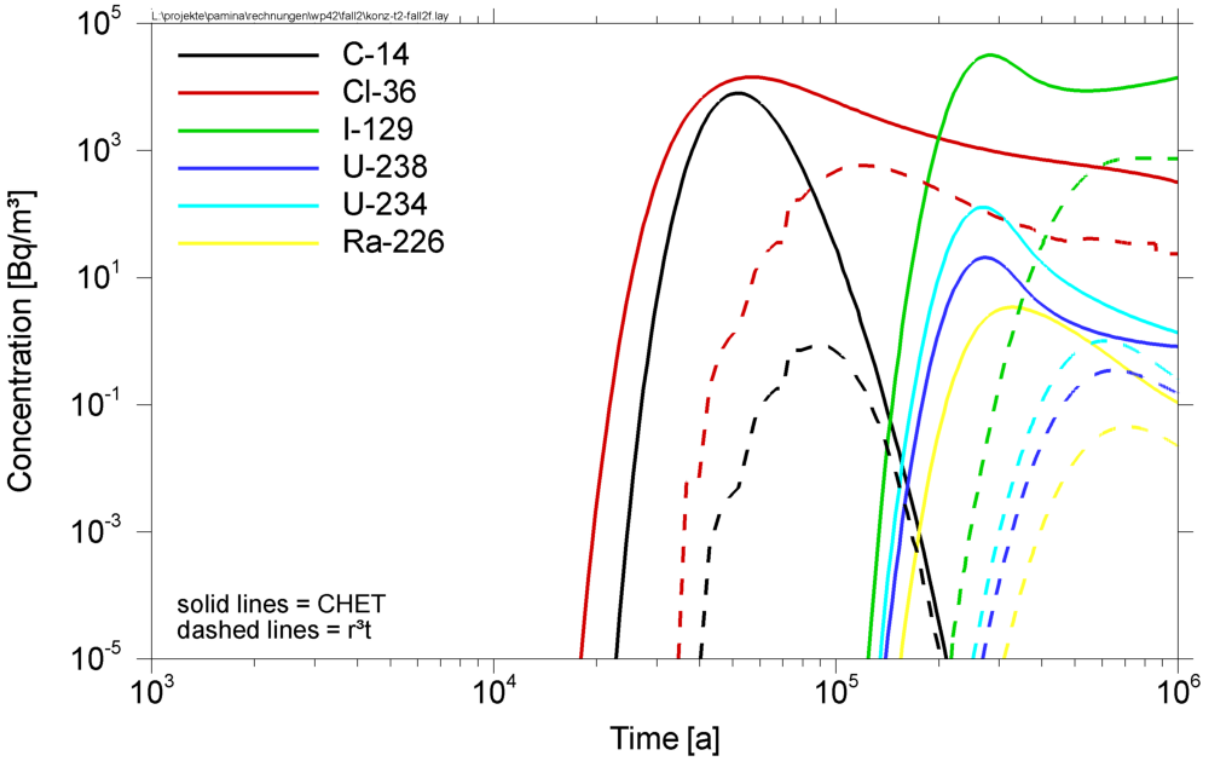

Fig. 24: Concentraton versus time of different radionuclides at the position of 12 650 m (pathway 2B) calculated with r^3t (dashed lines) and with high flow velocity used in CHET (solid lines)

7. Conclusions

In the work presented in this report, GRS examined the use of more complex far-field codes in PA. The GRS defined two generic test cases, both giving a very highly simplified representation of the situation found in the overburden above a real salt dome in Germany. For given radionuclide release rates from the near field there were performed transport calculations for both test cases, once with the 1D PA code CHET and once with the 2D codes d^3f and r^3t. As result of these calculations, the time dependent concentrations were compared at different positions in the model to study whether the use of the more complex codes results in a reduction of conservatism and/or a better representation of the actual transport or not.

On the one hand, with regard to processor time needed for the calculations, the use of the simplified code in PA is inevitable if multiple or even a high number of simulations have to be performed. The time for one simulation ranges from days to several weeks for the complex code r^3t versus only minutes for the PA code CHET. However, on the other hand, the simplification of the model brings along several peculiarities that have to be considered. The results are shortly outlined in the following five bullets:

- The radionuclide distribution calculated with the 2D code r^3t shows that different radionuclides can be transported on different transport pathways depending on their transport properties. This implies that the transport cannot be depicted by a single 1D model in these cases.
- The fraction of the radionuclides transported on one or the other of the different pathways differs from nuclide to nuclide.
- The missing dispersion to the second dimension results in an overestimation of the concentrations in the 1D model versus the 2D model. This effect is increasing with decreasing flow velocity and is most significant for diffusion dominated transport. The same deviation is expected between the 2D simulation and one using a 3D geometry.
- The heterogeneity of the transport velocities in the real situation and the need for averaging the velocities for the abstraction to 1D may result in large uncertainties on how to determine the correct transport velocity in the abstracted model. The deviation resulting from the averaging can lead to too high transport velocities and therefore an overestimation of the radionuclide concentrations in the aquifer water as observed in model 1, but also in too low transport velocities and resulting underestimations of the radionuclide concentrations as observed in model 2. The latter case is critical for safety assessment.
- A fast transport at the end of the transport pathway in a 1D model can result in an underestimation of the concentration of daughter radionuclides produced from the decay chains during the transport due to lacking residence time to equilibrate the decay chain.

Especially the first one and the last to points have to be considered in PA calculations since they can lead to an underestimation of the radiological consequences what absolutely has to

be avoided. The last point is quite common in PA radionuclide transport modelling and can be easily accounted for by considering an additional transport time in the 1D model that gives time to achieve the radioactive equilibrium in the decay chains.

The problem how to calculate average transport velocities for the abstracted model is more serious and a common solution is hard to recommend. One solution is to use the maximum transport velocity occurring in the real situation (i.e. the complex model). However, this approach in most cases might lead to a high conservatism in the model. Since the trend in latest safety assessments in European countries is towards neglecting a barrier function of the far-field anyway, this limitation might not be too harmful.

In cases where the far-field is regarded as barrier in the safety assessment and the hydrogeology shows a very complex flow field, a two-stage approach is needed. In a first step the more complex code and model is used to calculate the concentration distributions and consequences for a reference case. In the second step the results from the complex code are used to qualify the abstracted transport model and to show that the abstracted model does not underestimate the result. Subsequently, the abstracted model can be used for additional PA calculations like variants or probabilistic assessments.

In cases where radionuclides are transported on different pathways resulting in contamination of the surface water at different locations, the maximum radiation exposure cannot be correctly determined with a simple one dimensional model. However, this problem can be easily overcome by using a "multi 1D model", i.e. to model the different pathways independently with the 1D model and combine the results afterwards. This approach is shown exemplarily in figure 25 for the two pathways in model 1.

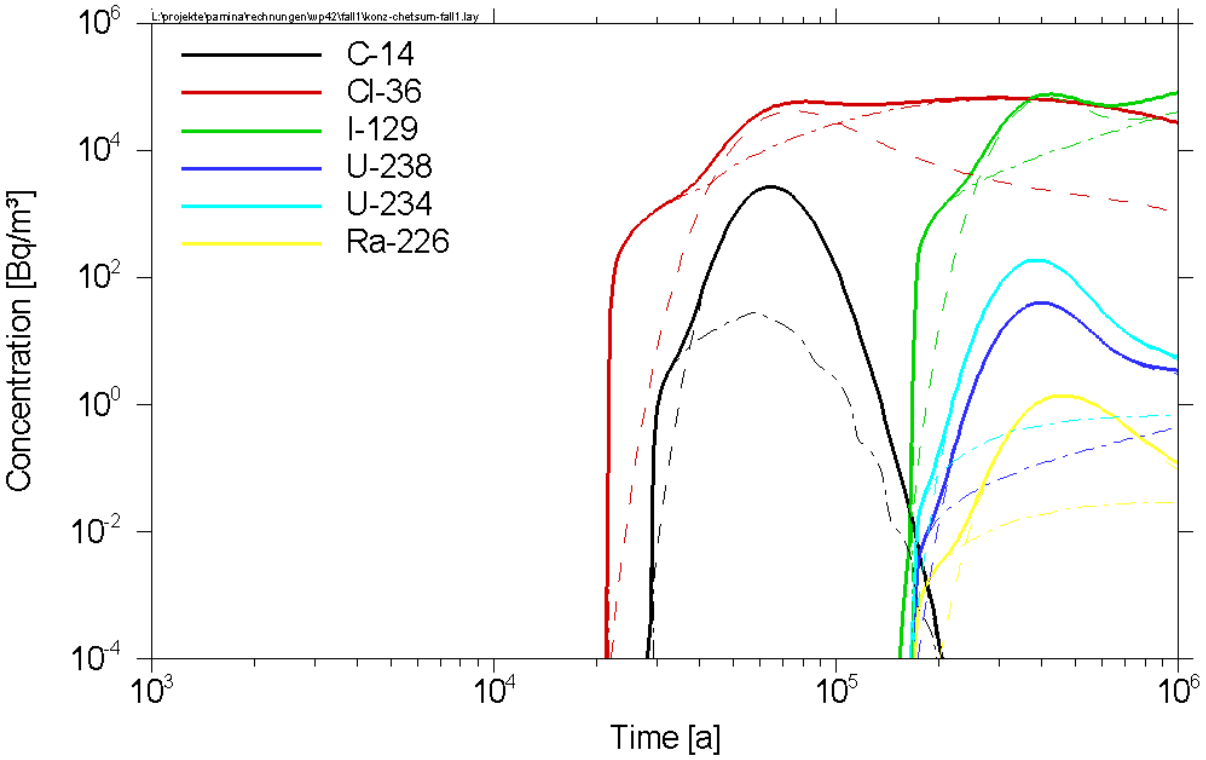

Fig. 25: Summed concentrations (solid lines) and respective contributions from both individual pathways (dashed and dash-dotted lines) calculated with the 1D model for model 1

8. Literature:

[1] Buhmann, D.: Das Programmpaket EMOS. Ein Instrumentarium zur Analyse der Langzeitsicherheit von Endlagern. Gesellschaft für Anlagen- und Reaktorsicherheit (GRS) mbH, GRS-159, Braunschweig, 1999.

[2] Fein, E.; Schneider, A.: d^3f - Ein Programmpaket zur Modellierung von Dichteströmungen. Gesellschaft für Anlagen- und Reaktorsicherheit (GRS) mbH, GRS-139, Braunschweig, 1999.

[3] Fein, E.: Software Package r3t. Model for Transport and Retention in Porous Media. Final report. Gesellschaft für Anlagen- und Reaktorsicherheit (GRS) mbH, GRS-192, Braunschweig, 2004.

[4] Flügge, J.: Radionuclide Transport in the Overburden of a Salt Dome – The Impact of Extreme Climate States, Dissertation, Technische Universität Carolo-Wilhelmina zu Braunschweig, 2009.

[5] Klinge, H.; Boehme, J.; Grissemann, C.; Houben, G.; Ludwig, R.R.; Rübel, A.; Schelkes, K.; Schildknecht, F.; Suckow, A. (2007): Standortbeschreibung Gorleben: Die Hydrogeologie des Deckgebirges des Salzstocks Gorleben. Geologisches Jahrbuch, Reihe C, Band 71, E.Schweizerbart'sche Verlagsbuchhandlung, Stuttgart.

[6] Keesmann, S.; Noseck, U.; Buhmann, D.; Fein, E.; Schneider, A.: Modellrechnungen zur Langzeitsicherheit von Endlagern in Salz- und Granitformationen. Gesellschaft für Anlagen- und Reaktorsicherheit (GRS) mbH, GRS-206, Braunschweig 2005.

[7] Kühle, T.; Zude, F.; Lührmann, L.: Das eindimensionale Transportprogramm CHET1 unter Berücksichtigung der Sorption nach dem Kd-Konzept. Gesellschaft für Anlagen- und Reaktorsicherheit (GRS) mbH, GRS-124, Braunschweig 1996.

[8] Schelkes, K.: Modelluntersuchungen zur Bewegung des Grundwassers bei vom Salzgehalt abhängiger Wasserdichte - Fallstudien und Modellvalidierung im Hinblick auf die Langzeitsicherheit von Endlagern für radioaktive Abfälle -. Abschlußbericht zum Forschungsvorhaben 02 E 8301. Bundesanstalt für Geowissenschaften und Rohstoffe, Hannover 1995.

[9] Suter, D.; Biehler, D.; Blaser, P.; Hollmann, A.: Derivation of a Sorption Data Set for the Gorleben Overburdon. Proc. DisTec ’98 International Conference on Radioactive Waste Disposal, S.581-584, Hamburg, 1998.